molecular pharmaceutics

Article

pubs.acs.org/molecularpharmaceutics

Paclitaxel-Loaded *N*-Octyl-*O*-sulfate Chitosan Micelles for Superior Cancer Therapeutic Efficacy and Overcoming Drug Resistance

Xiang Jin,[†] Ran Mo,[†] Ya Ding,*[,†] Wei Zheng,[‡] and Can Zhang*[,†]

[†]State Key Laboratory of Natural Medicines, Center of Drug Discovery, China Pharmaceutical University, 24 Tong Jia Xiang, Nanjing 210009, China

[‡]School of Life Sciences, State Key Laboratory of Pharmaceutical Biotechnology, Nanjing University, 22 Han Kou Road, Nanjing 210093, China

Supporting Information

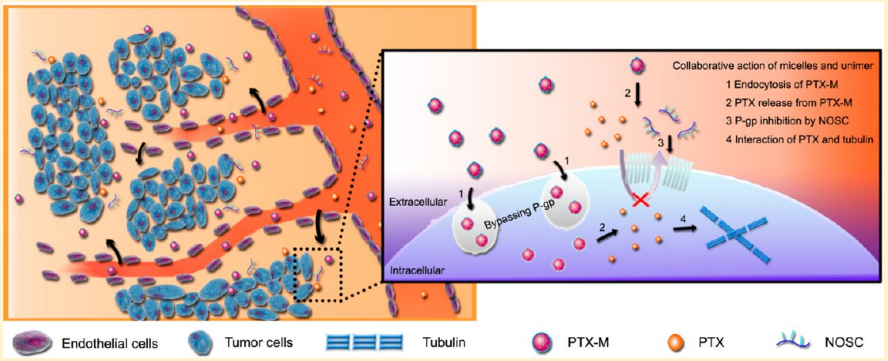

ABSTRACT: The nanoparticle-based drug delivery system holds great attraction to overcome or circumvent multidrug resistance (MDR) in cancer to date. In this work, a synthesized amphiphilic graft copolymer, *N*-octyl-*O*-sulfate chitosan (NOSC), and its paclitaxel (PTX)-encapsulated micelles (PTX-M) have been systematically investigated on the MDR reversal effect *in vitro* and *in vivo* as well as the mechanism of P-glycoprotein (P-gp) inhibition. NOSC in a wide concentration range even above the critical micelle concentration showed an effective effect on inhibiting P-gp-mediated PTX efflux, which was remarkably different from the surfactants and the Pluronic copolymers. Multiple mechanisms were involved in this effect of NOSC, such as stimulating P-gp ATPase, competitively impeding the binding of PTX with P-gp and reducing the fluidity of the cell membrane. PTX-M presented the highest cellular uptake and the lowest efflux rate of PTX, thereby yielding the optimal cytotoxicity on both the human hepatocellular liver carcinoma (HepG2) cells and the multidrug resistance HepG2 (HepG2-P) cells, which resulted from a combination of the inhibiting P-gp effect of NOSC and the bypassing P-gp action of the intact PTX-M. Additionally, PTX-M had superior blood persistence, tumor accumulation, and therapeutic efficacy after intravenous injection into the tumor-bearing mice. Furthermore, it was demonstrated that most of PTX-M as an intact form was delivered at the tumor site, which ensures the synergetic effect of NOSC micelles on drug delivery and P-gp inhibition. The aforementioned results suggested that NOSC micelles presented promising potential as an anticancer drug carrier for enhanced MDR cancer therapy.

KEYWORDS: *N-octyl-O-sulfate chitosan, micelle, paclitaxel, P-gp inhibition, drug resistance*

INTRODUCTION

Multidrug resistance (MDR), often found in many types of human cancer,[1] is one of the crucial factors for the low efficiency of cancer chemotherapy,[2] which leads to the drug steady-state level lower than the therapeutic window in the tumor tissues and therefore the relapse of the tumor after an initial favorable response to drug therapy. The process of MDR generally involves the activity of P-glycoprotein (P-gp), which functions as an ATP-dependent efflux pump to drain the chemotherapeutics out of the cells.[3,4] The current approach used to overcome MDR in the cancer cells is a coadministration of antineoplastics with agents that can modulate P-gp activities such as verapamil, cyclosporine A, and its analogues.[5−7] Moreover, a number of surfactants including Cremophor EL, Tween 80, and D-α-tocopheryl polyethylene glycol 1000 succinate (TPGS) have been reported to enhance the transport of drugs across the human colon carcinoma (Caco-2) cell monolayer by inhibiting an apically polarized efflux system.[8−10] Recently, nanomedicine, typically a nanoparticle-based drug delivery system (DDS), has attracted significant attention for the MDR reversal in cancer treatment, such as nanoparticles,[11−13] liposomes,[14] and polymeric micelles.[15−19] The mechanisms of the MRD reversal contain the specific targeting,

Received: June 10, 2013
Revised: October 15, 2013
Accepted: November 21, 2013
Published: November 21, 2013

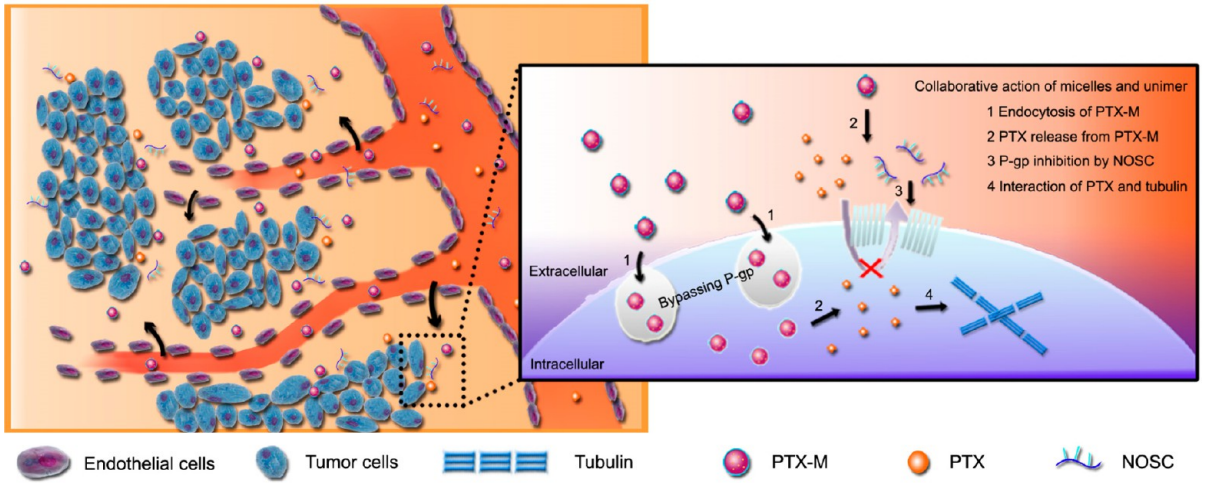

Figure 1. Scheme of collaborative mechanism-induced improvement on the PTX-resistant cellular uptake and therapeutic efficacy of PTX by PTX-M: passive targeting of the intact PTX-M to the tumor tissues by the EPR effect (A) and the mechanism of enhanced accumulation of PTX inside tumor cells by PTX-M *via* a combination mechanism of the inhibiting P-gp effect of NOSC and the bypassing P-gp action of the intact PTX-M (B).

the enhanced cellular uptake, and the increased bioavailability of drugs *via* the improved physicochemical and pharmacokinetic characteristics of nano-DDSs.[20,21]

Of note, it would be a simple and effective approach to improve the MDR reversal in combination with the existing therapies in the case that the components of the nanocarriers possess the P-gp inhibition capability.[12−14,16,17] For example, the Pluronic block copolymer showed a strong effect on P-gp inhibition below its critical micelle concentration (CMC).[22,23] Although the exact mechanism is not clear yet, the ability of the Pluronic copolymer to block the P-gp activity is potentially associated with the interaction of the individual copolymer chains with P-gp to reduce the ATPase activity or interfere with the lipid microenvironment surrounding P-gp.[18,19] However, it is worth noting that the P-gp inhibition effect of the Pluronic copolymers attenuated and even disappeared accompanied by the formation of the self-assembled micelles at the concentration higher than the CMC,[22,23] thereby resulting in a decent of their roles in the studies of overcoming MDR. Accordingly, the exploitation of DDSs with the desirable pharmaceutical properties as well as an excellent P-gp inhibition function is highly appealing and remains challenging.

Paclitaxel (PTX) is a mitotic inhibitor with a good antitumor activity but a poor water solubility. As a substrate of P-gp, its antitumor efficacy is seriously influenced by MDR. Many formulations have already been exploited to solve the problems of the poor solubility and the unspecific biodistribution of PTX. Thereinto, Cremophor EL, a constituent in Taxol, has also been reported to inhibit the P-gp efflux of PTX.[8] However, the severe side effects of Cremophor EL were determined after intravenous administration of Taxol, including anaphylactoid hypersensitivity reactions, hyperlipidaemia, abnormal lipoprotein patterns, aggregation of erythrocytes, and peripheral neuropathy.[24] To address these issues, the Cremophor-free formulations such as Abraxane (albumin-bound PTX nanoparticles), Lipusu (liposomal PTX), and Genexol-PM (PTX poly(ethylene glycol)−polylactide (PEG-PLA) micelles) have been developed to eliminate the solvent-related toxicities.[25] Despite the reduced systematic toxicity of these Cremophor-free formulations compared with Taxol, they are not efficient for the MRD tumor treatment,[23] and no MDR reversal effects are reported. In our previous work, *N*-octyl-*O*-sulfate chitosan (NOSC)[26] has been synthesized to construct etoposide- or PTX-encapsulated micelles for increased oral absorption and bioavailability.[27,28] The cellular uptake of micelles compared with the free drugs showed an enhanced efficiency in Caco-2 cells, and the possible P-gp inhibition effect of NOSC was speculated.

In this work, we are highly interested in the MDR reversal activity of NOSC micelles and the mechanism of P-gp inhibition as well as the enhanced therapeutic efficacy of PTX-loaded NOSC micelles (PTX-M) on chemotherapy-resistant cancer. As shown in Figure 1, unlike the Pluronic micelles, NOSC micelles presented anti-MDR capability in a wide polymer concentration range even above the CMC. The related mechanism was extensively explored such as the impact of NOSC and its micelle on the cellular uptake, the expression of P-gp, ATPase activity of P-gp, the affinity of PTX with P-gp, the fluidity of cell membrane, and the expression and the activity of glutathione S transferase (GST). Based on the distinctive property of NOSC and its micelle, PTX-M showed a superior anticancer efficacy compared with free PTX, Taxol, and the physical mixture of Taxol with the same concentration of NOSC, especially in the PTX-resistant human hepatocellular carcinoma (HepG2-P) cells and their tumor xenograft mouse model. It provides the evidence that the exploitation of polymeric nanocarriers possessing anti-MDR capability would be a more simple and effective strategy to improve the therapeutic efficacy on the MDR tumor.

EXPERIMENTAL SECTION

Materials. *Chemicals.* Paclitaxel was purchased from Yew Pharmaceutical Co. (Jiangsu, China). Verapamil was a gift from Hengrui Pharmaceutical Co. (Jiangsu, China). Sodium azide and Nile red were provided by Sigma-Aldrich (Shanghai, China). Cremophor EL was obtained from BASF (Germany). 3-[4,5-Dimethylthiazol-2-yl]-2,5-diphenyl tetrazolium bromide (MTT) was offered by Amresco (Solon, Ohio, USA). The BCA Protein Assay Kit and cell lysis buffer for Western and IP were purchased from Beyotime Institute of Biotechnology (Jiangsu, China). Antihuman CD243 (ABCB1) PE and mouse IgG2a κ isotype control functional grade purified were purchased from eBioscience (San Diego, CA). P-gp-Glo assay system with P-gp was bought from Promega Co. (Madison, USA). Fluorescein

Table 1. k_0 and k Values for HepG2 and HepG2-P Cells in Kinetic Study of Cellular Uptake

	HepG2 cells		HepG2-P cells	
formulation	k_0 (μg/h)	k (h^{-1})	k_0 (μg/h)	k (h^{-1})
Taxol	8.90 ± 1.23[b]	1.88 ± 0.15[a]	8.54 ± 1.22[b]	4.08 ± 1.24[a]
Taxol + NOSC	12.41 ± 1.14	1.49 ± 0.21	7.50 ± 1.64	1.35 ± 0.22[c]
PTX-M	28.46 ± 2.36	0.94 ± 0.04	22.90 ± 2.41	1.01 ± 0.18

[a] $P < 0.05$. [b] $P < 0.01$ vs PTX-M. [c] $P < 0.05$ vs Taxol.

isothiocyanate (FITC) was supplied by JingKeHongDa Biotechnology Co., Ltd. (Beijing, China). Other chemicals and solvents were analytical grade.

Cell Lines. The human hepatocellular carcinoma (HepG2) cells were provided by the cell bank of Chinese Academy of Sciences. HepG2-P cells were obtained from Wuhan University. The cells were cultured in RPMI-1640 cell culture medium containing 10% (v/v) FBS, 100 IU/mL penicillin, and 100 μg/mL streptomycin at 37 °C under 5% CO_2.

Animals and Tumor Xenografts. Male Institute of Cancer Research (ICR) mice (18−20 g) were purchased from College of Veterinary Medicine Yangzhou University (Jiangsu, China). The experiments were carried out in compliance with the Guide for Care and Use of Laboratory Animals approved by local committee. Hepatoma solidity (Heps) cells provided by Nanjing University were maintained in ascites in ICR mice, while PTX-resistance Heps cells (Heps-P) were cultured by our group and saved in ascites in ICR mice. The mice were subcutaneously inoculated in the back with the cancer cells (1×10^7 cells/mouse) to set up the tumor xenograft model. The tumor size was monitored by a fine caliper, and the tumor volume (V) was calculated as $V = L \times W^2/2$, where L and W were the length and width of the tumor, respectively.

Synthesis of NOSC and Preparation of PTX-M. NOSC (chemical structure shown in Figure S1, Supporting Information) and PTX-M were prepared by our group as previously described.[28] NOSC was synthesized using chitosan with a viscosity average molecular weight of 65−70 kDa, and the substitutions of the octyl degree and the sulfonic degree were 0.38 and 2.56, respectively. The CMC of NOSC micelles was about 0.045% (w/v). PTX-M was prepared by the dialysis method. The drug-loading rate of PTX-M was about 40% with the feeding ratio of PTX:NOSC as 1:1 (w/w), and the PTX concentration in PTX-M was approximately 2.5 mg/mL with the NOSC concentration of 0.4% (w/v) (Table 1, Supporting Information).[28] It is important to note that two kinds of PTX-M formulations were used in the following studies. In the investigations on cellular uptake and P-gp inhibition mechanism, we reduced the feeding ratio of PTX:NOSC to 1:4 (w/w) and prepared PTX-M with the PTX concentration of 0.5 mg/mL and the NOSC concentration of 0.4% (w/v), which ensured that the diluted PTX and NOSC concentrations in PTX-M were consistent with that in the physical mixture of Taxol and NOSC (Taxol + NOSC). For the *in vitro* cytotoxicity and *in vivo* animal studies, PTX-M containing 2.5 mg/mL PTX and 0.4% (w/v) was used to evaluate its anticancer activity.

Cellular Uptake Studies. *NOSC Concentration Effect on the Cellular Uptake of PTX.* HepG2 and HepG2-P cells (1×10^5 cells/well) were seeded in 24-well plates. After 80% overspread, the cells were incubated with different formulations containing the same amount of PTX (2.5 μg/mL) at 37 °C for 8 h. The formulations were listed as follows: (1) PTX dissolved in the cell culture medium containing 1% DMSO (v/v); (2) PTX + verapamil (100 μM); (3) PTX + NOSC (0.008%, 0.04%, and 0.08%, w/v, denoted as the respective concentrations lower than, equal to, and higher than the CMC of NOSC micelles); PTX + Cremophor EL (0.01% and 0.1%, w/v). Afterward, the formulations were removed, and the cells were washed by ice-cold PBS thrice. The amount of PTX in cells was determined by high-performance liquid chromatography (HPLC), which was calculated as $U_{PTX} = Q_{PTX}/Q_{protein}$, where Q_{PTX} and $Q_{protein}$ were the amounts of PTX and cellular protein, respectively.

Mechanisms of Cellular Uptake. HepG2-P cells were incubated with Taxol and PTX-M containing the same amount of PTX (50 μg/mL) at 37 °C for 8 h. To investigate the cellular uptake as a energy-dependent process, the incubation temperature was reduced to 4 °C, or a energy inhibitor (0.1% sodium azide) was added to the cells prior to incubation, respectively. After incubation, the test solutions were removed, and the cells were washed by ice-cold PBS thrice. The amount of PTX in HepG2-P cells was assayed by HPLC.

Kinetics of Cellular Uptake. HepG2 and HepG2-P cells (1×10^5 cells/well) were seeded in 24-well plates. After 80% overspread, the cells were incubated with different formulations containing the same amount of PTX (100 μg/mL) at 37 °C. The formulations were listed as follows: (1) Taxol; (2) Taxol + NOSC (0.08%, w/v); (3) PTX-M. At predetermined incubation time intervals, the cells were washed by cold PBS thrice, and the amount of PTX in cells was assayed by HPLC.

P-gp Inhibition Mechanism. *P-gp Expression.* To evaluate the effect of NOSC on the P-gp expression, the P-gp-antibody binding assay kit with Anti-Human CD243 (ABCB1) PE as a P-gp monoclonal antibody was used to measure the amount of P-gp expression in HepG2-P cells.[29] HepG2-P cells (1×10^6 cells/well) were seeded in 6-well plates. After for 80% overspread, the cells were incubated with different formulations at 37 °C for 8 h. The formulations were listed as follows: (1) verapamil (100 μM); (2) NOSC (0.008%, 0.04% and 0.08%, w/v); (3) FBS free culture medium as a control. Subsequently, the cells were washed by ice-cold PBS thrice and collected by centrifugation at 1000 × g for 5 min. A portion of 100 μL of each cell suspension was added with antihuman CD243 (ABCB1) PE solution (5 μL, 0.5 μg) and mouse IgG2a κ isotype control PE solution (5 μL), respectively, and incubated in dark at room temperature for 30 min. After removing the extracellular PE by centrifuge and washing with ice-cold PBS thrice, the cells were analyzed using flow cytometry (BD FACSCalibur). The fluorescence intensity reflected the P-gp expression on cells. The amount of P-gp expression in HepG2 cells was taken as a reference.

P-gp ATPase Activity. To evaluate whether the effect of NOSC on P-gp was connected with interfering P-gp ATPase, the Pgp-Glo assay system with P-gp was used, which can detect the impact of compounds on recombinant human P-gp in a cell membrane fraction. The assay depended on the ATP dependence of the light-generating reaction of firefly luciferase, which was detected by a Modulus single tube multimode reader

(Turner Biosystens, Sunnyvale, CA). The test compounds were listed as follows: (1) NOSC (0.008%, 0.04%, and 0.08%, w/v); (2) Na_3VO_4 (100 μM, a selective inhibitor of P-gp), and verapamil (200 μM). The procedures of this experiment were performed in accordance with the manufacturer's protocol.

P-gp Binding Site. P-gp-rich membrane vesicles containing 10 μg of P-gp were incubated with 0.2 mL of P-gp binding buffer (50 mM Tris/HCl, pH 7.4) containing PTX (0.12 μM) and the mixture of PTX (0.12 μM) with different concentrations of NOSC and verapamil, in multiscreen 24-well plate 0.22 μm pore size (Millipore, USA) for 30 min at room temperature, respectively. The binding reaction was stopped by adding 0.25 mL of ice-cold wash buffer (20 mM Tris/HCl, 50 mM $MgSO_4$, pH 7.4). All of the samples were rapidly filtered, and the amount of PTX entrapped on filters was detected by HPLC.

Membrane Fluidity Studies. A suspension of HepG2-P cells was washed by PBS thrice and incubated with the 1,6-diphenyl-1,3,5-hexatriene (DPH) labeling solution (2 mM) at 37 °C for 1 h. The cells were then washed by PBS thrice to remove extracellular DPH. The suspension of the labeled cells was mixed with NOSC solutions (0.008%, 0.04%, and 0.08%, w/v) and incubated at 37 °C for 1 h under gentle stirring. Cholesterol (0.2 mM) was used as a negative control. Fluorescence anisotropy was then measured at the excitation/emission wavelength of 360 nm/430 nm by an SLM-AMINCO subnanosecond lifetime fluorometer (model 4800c) at room temperature. The microviscosity of the membrane hydrophobic area was calculated according to the Perrin equation as described in detail elsewhere.[30]

GSH Assay. The levels of the intracellular reduced glutathione (GSH) were determined in HepG2-P cells. The cells after 1 h of incubation with different concentrations of NOSC (0.008%, 0.04%, and 0.08%, w/v) were lyzed by 4% trichloracetic acid. Following the removal of the precipitated protein by centrifugation at 10000 rpm for 10 min, the supernatants were neutralized by sodium hydroxide (NaOH). A sample of 0.5 mL of the supernatant was added to 1 mL of Ellman's reagent (16 mg of dinitro-5-thiobenzoic acid in 0.1 M sodium phosphate (pH 8.0)). The absorbance was assayed at 412 nm by a spectrophotometer (UV-3600, SHIZUMA, Japan).

GST Assay. The influence of NOSC on GST activity in HepG2-P cells was determined using a GST Fluorometric Activity Assay Kit (Biovision, USA). After incubation with different concentrations of NOSC (0.008%, 0.04%, and 0.08%, w/v) for 1 h, the cells were washed with ice-cold PBS twice, lyzed in 1.0% Triton X-100, and centrifuged at 10000 rpm for 15 min. The following procedures were in performed in accordance with the manufacturer's protocol.

Cytotoxicity Studies. The *in vitro* cytotoxicity of different PTX formulations was determined by a MTT assay. Briefly, HepG2 and HepG2-P cells (1×10^4 cells/well) were seeded in 96-well plates for 24 h and incubated with different PTX formulations including (1) PTX; (2) Taxol; (3) Taxol + NOSC; (4) PTX-M. The concentration of NOSC added with Taxol was consistent with that in PTX-M formulation. After 48 or 72 h of incubation, 20 μL of the MTT solution (5 mg/mL) was added to each well, and the cells were stained at 37 °C for 4 h. Then the medium was removed, and the cells were dissolved in 150 μL of dimethyl sulfoxide (DMSO). The medium was then washed out by PBS, and the cells were mixed with 150 μL of DMSO. The absorbance was measured at 570 nm by an enzyle-linked immunosorbent assay (ELISA) (Thermo Scientific, USA). The half maximal inhibitory concentration (IC_{50}) was calculated using nonlinear regression analysis.

Animal Studies. *In Vivo Antitumor Efficacy.* When the tumor volume reached 0.1 cm^3, the Heps-P tumor-bearing mice were weighed, randomly divided into four groups, and intravenously administrated with (1) Taxol; (2) Taxol + NOSC (0.08%, w/v); (3) PTX-M; and (4) saline as a negative control at the PTX dosage of 20 mg/kg at day 3, 5, 7, 9, and 11. At day 21, the tumor were harvested from the mice after euthanasia, washed by saline thrice, and then fixed in 10% neutral buffered formalin (NBF). For hematoxylin and eosin (H&E) staining, formalin-fixed tumors were embedded in paraffin blocks and visualized by an optical microscope (Olympus, Japan).

Intratumoral Accumulation and Localization of PTX-M. Tumor-bearing mice were randomly assigned to six groups (three groups for xenograft Heps cells and the other three groups for xenograft Heps-P cells). After intravenous injection by different PTX formulations, the tumor-bearing mice were euthanized at 0.0833, 0.25, 0.5, 1, 2, 4, and 8 h postinjection. The tumor was collected, weighed, and stored at −20 °C until HPLC analysis.

For observation of the location of the NOSC micelles at the tumor site, Nile red (Nr) was coencapsulated with PTX in the FITC-modified NOSC micelles to prepare dual-fluorescent-labeled PTX-M. Briefly, FITC-NOSC was dissolved in the distilled water, while Nr with PTX was dissolved in dehydrated ethanol; the other procedure for the preparation of FITC- and Nr-labeled PTX-M (FITC/Nr-M) was similar to that of PTX-M. FITC/Nr-M was intravenously administrated to the Heps-P tumor-bearing mice. Tumor was collected after 8 h administration, washed with PBS, and treated by freezing microtomy and visualized by confocal laser scanning microscope (CLSM) (Leica TCS SP5, Germany). Hoechst 33258 was used for nuclear counterstaining.

PTX Quantification in Cells and Tissues. *Cell Sample Pretreatment Method.* Briefly, the cells in plates were disrupted by 180 μL of the cell lysis buffer to release the drug in the cells. After centrifugation at 10000 × *g* for 5 min, 20 μL of the supernatant was used for the BCA protein assay to quantitate the cell protein. In addition, the isovolumetric methanol was added into 100 μL of the supernatant for protein precipitation, vortexed for 5 min, and centrifuged at 10000 × *g* for 10 min. A sample of 20 μL of the supernatant was applied to HPLC.

Tumor Tissue Pretreatment Method. The weighed tissues were added by 800 μL of saline, followed by homogenation. A portion of 200 μL of the tissue homogenate was mixed with 200 μL of acetonitrile, vortexed for 5 min, and centrifuged at 10000 × *g* for 10 min. Twenty μL aliquots of the supernatant were applied to HPLC. The pharmacokinetic parameters were calculated by WinNonlin Noncompartmental Analysis (Version 5.2.1).

HPLC Assay. An HPLC assay was performed with an Shimadzu 2010AT system. The mobile phase consisted of methanol and water (75:25, v/v). A C_{18} column (250 mm × 4.6 mm × 5 μm, Diamonsil, China) was employed for the separation of analytes at a flow rate of 1 mL/min. The detection wavelength was set at 227 nm, and the column temperature was 35 °C.

Data Analysis. Data are expressed as the mean ± standard deviation, and statistical analysis was performed by SPSS. *P <

0.05 was considered significant, and $^{**}P < 0.01$ was extremely significant.

RESULTS

Cellular Uptake Studies. *Effect of NOSC on the Cellular Uptake of PTX.* The intracellular amount of PTX influenced by the concentration of NOSC was evaluated in HepG2 and HepG2-P cells, respectively. For a meaningful comparison, the cellular uptake of free PTX was shown in Figure 2 in the absence and presence of a P-gp inhibitor (verapamil) or a surfactant that has P-gp inhibition effect (Cremophor EL) as a control. In HepG2 cells, the average cellular uptake of PTX in the presence of verapamil was 1.60-fold that of free PTX, which indicated that the P-gp inhibitor can effectively reduce the PTX efflux by P-gp. The presence of Cremophor EL with a low concentration (0.01%, w/v) also improved the cellular uptake of PTX in HepG2 cells, which was 1.65-fold that of free PTX. However, when the Cremophor EL concentration increased to 0.1% (w:v), the cellular uptake amount (684.5 ± 231.8 ng/mL) was comparable to that of the free PTX (604.2 ± 187.9 ng/mL). Of note, the presence of NOSC at different concentrations (0.008%, 0.04%, and 0.08%, w/v) traversing the CMC of NOSC (0.45%, w/v) promoted the cellular uptake of PTX, which was calculated to be 1.54-, 1.60-, and 1.53-fold that of free PTX, respectively.

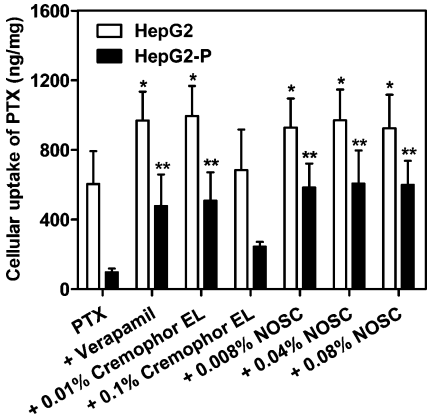

Figure 2. Effect of NOSC with different concentrations on the cellular uptake of PTX in HepG2 and HepG2-P cells. $^{*}P < 0.05$ vs PTX. $^{**}P < 0.01$ vs PTX.

On the part of HepG2-P cells, due to the high expression level of P-gp at the cell surface, the cellular uptake of PTX by all of the formulations displayed a decline in varying degrees, especially for the free PTX group (decreased by 6.3 times). Other groups with the help of verapamil, Cremophor EL, and NOSC in HepG2-P cells showed the similar trend of enhanced cellular uptake of PTX that was determined in HepG2 cells above. However, it is worth noting that NOSC with different concentrations showed the highest PTX uptake in HepG2-P cells in contrast to in HepG2 cells. The cellular uptake of PTX with the NOSC concentrations of 0.008%, 0.04%, and 0.08% (w/v) were detected to be 583.25 ± 138.33, 605.16 ± 192.11. and 598.46 ± 139.02 ng/mg in HepG2-P cells, respectively, which equal about 6.0-fold, 6.3-fold, and 6.2-fold that of free PTX control, respectively.

Mechanisms of Cellular Uptake. To confirm the active internalization of PTX-M by HepG2-P cells, the cellular uptake of PTX was shown in Figure 3 after the cells were incubated with PTX-M at 37 °C, at 4 °C, or in the presence of sodium azide at 37 °C. Taxol containing the same amount of PTX with PTX-M was taken as a control. It was shown that the cellular uptake of PTX-M was remarkably higher than that of Taxol at 37 °C. More importantly, both of the metabolic (low temperature, 4 °C) and chemical (sodium azide) energy inhibitors had no obvious impact on the cellular uptake of PTX in Taxol, whereas the cellular uptake of PTX by PTX-M was significantly reduced. The cellular uptake of PTX-M at 37 °C was 22.40 ± 1.91 μg/mg, much higher than that at 4 °C (3.62 ± 0.18 μg/mg) or that at 37 °C in the presence of sodium azide (8.92 ± 0.33 μg/mg).

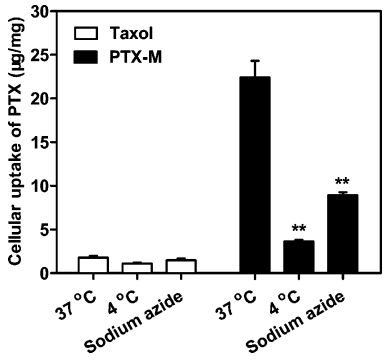

Figure 3. Cellular uptake mechanism of PTX-M: the effect of the low temperature, 4 °C, and the chemical energy inhibitor, sodium azide, on the cellular uptake of Taxol and PTX-M in HepG2-P cells. $^{**}P < 0.01$ vs control (37 °C).

Kinetics of Cellular Uptake. The intracellular PTX amount in HepG2 and HepG2-P cells delivered by different PTX formulations over time was shown in Figure 4. In HepG2 cells, Taxol showed the lowest PTX content during the experimental period from 30 min to 8 h. With the addition of NOSC with a concentration (0.08%, w/v) higher than the CMC, the PTX content inside the cells at 30 min was close to that of the Taxol group. However, as time increased, the intracellular PTX concentration gradually increased and reached 12.90 ± 0.83 μg/mg within 8 h, which was higher than that of Taxol (8.57 ± 2.12 μg/mg). As expected, PTX-M not only displayed the highest cellular uptake from the beginning of the assay but also showed a rapid cellular uptake rate, which had a cellular uptake of 9.31 ± 1.08 μg/mg almost 2-fold that of Taxol in the first 30 min, and a continuous accumulation of PTX into the cells remained. The maximum value (30.67 ± 2.50 μg/mg) was obtained after 8 h of cell incubation, which was 2.58 and 1.38

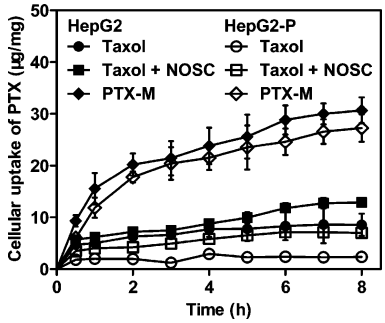

Figure 4. Cellular uptake of different PTX formulations including Taxol, Taxol + NOSC (0.08%, w/v), and PTX-M at a PTX concentration of 100 μg/mL over time.

dx.doi.org/10.1021/mp400340k | Mol. Pharmaceutics 2014, 11, 145−157

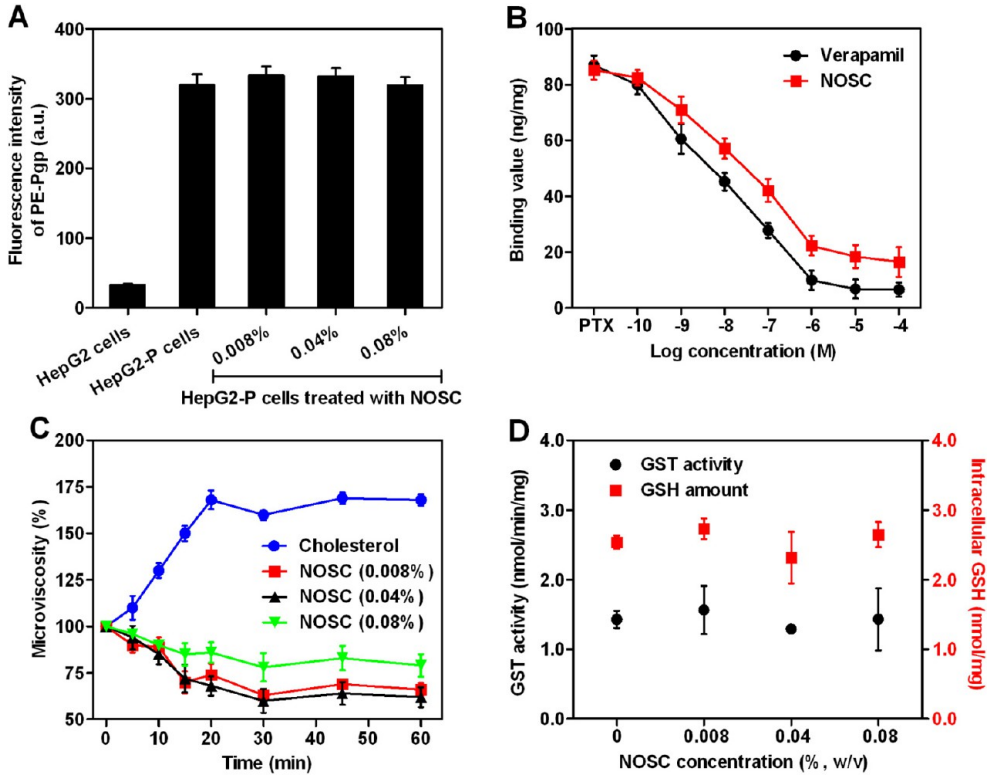

Figure 5. P-gp inhibition mechanism of NOSC and its micelles: the effect of NOSC on the P-gp expression (A), the binding of PTX with P-gp (B), the microviscosity of the plasma membrane (C), and the intracellular GST/GSH level (D).

higher than that of Taxol and Taxol + NOSC groups, respectively. In HepG2-P cells, the trends were consistent with that in HepG2 cells, although the cellular uptake values declined correspondingly in each group.

Based on the cellular uptake kinetics shown in Figure 4, the kinetic model was established, and it is shown in eq 1.

$$X = \frac{k_0}{k}(1 - e^{-kt}) \quad (1)$$

Assuming that the cellular uptake and elimination of PTX at a constant uptake speed (k_0) and efflux rate (k) at the same time, the values of k_0 and k were obtained through nonlinear fitting of data from cellular uptake kinetic results. As shown in Table 1, there was no significant difference between the k_0 values of Taxol in the absence and presence of NOSC regardless of the type of cells. However, the k_0 values of PTX-M in both HepG2 and HepG2-P cells were comparable but noticeably higher than those of Taxol with and without NOSC. In addition, the k value of Taxol in HepG2-P cells (4.08 ± 1.24 h^{-1}) was much higher than that in HepG2 cells (1.88 ± 0.15 h^{-1}), which indicated that a fast efflux rate of PTX in the cells with high level of P-gp expression was observed even under the protection of Cremophor EL. For the Taxol + NOSC group, the k value in the HepG2-P cells (1.35 ± 0.22 h^{-1}) slightly reduced to a level lower than that in the HepG2 cells (1.49 ± 0.21 h^{-1}). Furthermore, the k values of PTX-M in HepG2 and in HepG2-P cells were 0.94 ± 0.04 h^{-1} and 1.01 ± 0.18 h^{-1}, respectively, as the lowest values compared with that of other PTX formulations. Therefore, the cellular uptake kinetics of PTX by PTX-M showed the highest uptake speed (k_0) with the lowest drug efflux rate (k) within 8 h.

P-gp Inhibition Mechanism. To explore the P-gp inhibition mechanism of NOSC, a series of investigations were performed including the influence of NOSC on the expression of P-gp, the activity of P-gp ATPase, the binding site of PTX on P-gp, the fluidity of cell membrane, the intracellular amount of GSH, and the activity of GST.

The expression level of P-gp in HepG2-P cells was measured before and after the treatment of different concentrations of NOSC. As shown in Figure 5A, HepG2 cells showed a lower P-gp expression compared with HepG2-P cells as expected. After HepG2-P cells treated with NOSC, the expression levels of P-gp showed insignificant changes as the NOSC concentration increased from 0.008% to 0.08% (w/v).

Next, the effect of NOSC on the activity of P-gp ATPase was evaluated. As shown in Table 2, verapamil, a substrate for

Table 2. Influence of NOSC on P-gp ATPase (Mean ± SD, n = 3)[a]

sample	luminescence (RLU)	ΔRLU
untreated	721568 ± 35653	164880 ± 46298
Na_3VO_4 (100 μM)	886448 ± 66895	N/A
verapamil (200 μM)	347199 ± 78778[b]	539249 ± 48378[b]
NOSC (0.08%)	607242 ± 26528[c]	279206 ± 46848[c]
NOSC (0.04%)	512156 ± 50269[b]	374292 ± 24294[b]
NOSC (0.008%)	511070 ± 23774[b]	375379 ± 43912[b]

[a]Untreated (NT), 100 μM Na_3VO_4, 200 μM verapamil, and 0.008%, 0.04%, 0.08% NOSC-treated P-gp reactions were performed. Luminescence was read on a Modulus single tube multimode reader. The decrease in luminescence of NT samples compared to samples plus Na_3VO_4 (ΔRLU_{basal}) represents basal P-gp ATPase activity. The decrease in luminescence of verapamil-treated and NOSC-treated samples (ΔRLU_{TC}) represents the influence of verapamil and NOSC on P-gp ATPase, respectively. [b]$P < 0.01$, compared with the control. [c]$P < 0.05$, compared with the control.

dx.doi.org/10.1021/mp400340k | Mol. Pharmaceutics 2014, 11, 145−157

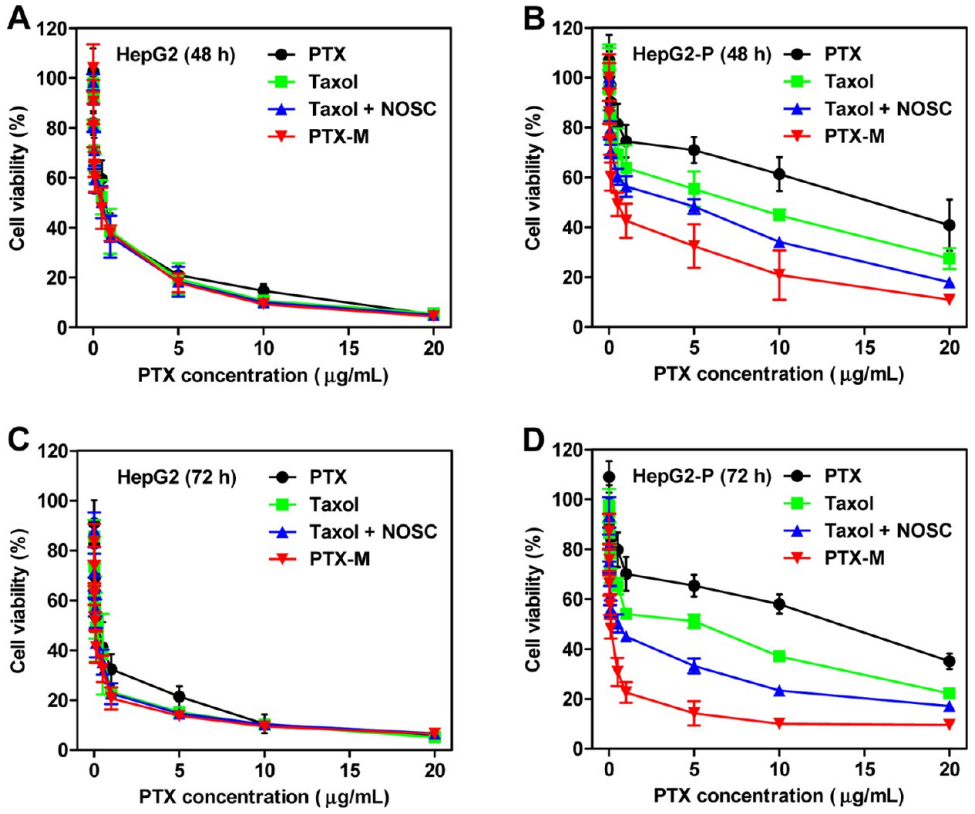

Figure 6. *In vitro* cytotoxicity of different PTX formulations toward HepG2 and HepG2-P cells for 48 h (A, B) and 72 h (C, D).

Table 3. IC_{50} and Resistance Reversion Index (RRI) of Various Formulations of PTX against HepG2 or HepG2-P Cells for 48 or 72 h

	HepG2 cells		HepG2-P cells			
formulation	IC_{50} (48 h) (μg/mL)	IC_{50} (72 h) (μg/mL)	IC_{50} (48 h) (μg/mL)	RRI[a]	IC_{50} (72 h) (μg/mL)	RRI
PTX	0.64 ± 0.04	0.21 ± 0.03	16.39 ± 3.22[b]		14.53 ± 0.32[b]	
Taxol	0.41 ± 0.02	0.13 ± 0.01	6.49 ± 1.14[b]	2.53	5.85 ± 0.72[b]	2.48
Taxol + NOSC	0.39 ± 0.03	0.07 ± 0.01	3.89 ± 0.24[b,c]	4.21	1.04 ± 0.24[b,c]	4.38
PTX-M	0.30 ± 0.03	0.05 ± 0.01	0.55 ± 0.23	29.63	0.08 ± 0.01	56.44

[a]RRI = IC_{50} (free PTX)/IC_{50} (other PTX formulations). [b]$P < 0.01$ vs PTX-M. [c]$P < 0.05$ vs Taxol.

transport by P-gp, can stimulate the P-gp ATPase activity. The positive relative light unit (RLU) value of verapamil (539249 ± 48378) demonstrated a strong stimulation effect on the P-gp ATPase, which resulted in the consumption of ATP by verapamil-stimulating P-gp.[31] NOSC with different concentrations also exhibited positive ΔRLU values, indicating that NOSC was also able to stimulate the P-gp ATPase activity with a similar P-gp inhibition mechanism to verapamil.[28]

In addition, the direct interaction of NOSC with P-gp had been investigated to disclose the possible binding site of NOSC on P-gp. As shown in Figure 5B, NOSC markedly inhibited the binding of PTX to P-gp, and this inhibition was concentration-dependent. The higher concentration of NOSC led to the weaker binding ability of PTX with P-gp. Verapamil also had the similar concentration-dependent effect on inhibiting the binding site of PTX with P-gp. It was suggested that the substrate of the drug transport protein could inhibit the transport of other molecules by P-gp in a competitive manner.[32]

To further validate whether the P-gp inhibition effect of NOSC is associated with disturbing the fluidity of the cell membrane, the impact of NOSC on the cell membrane structure was evaluated based on the fluorescence polarization using a hydrophobic fluorescent tracker, DPH.[30,33] The fluorescence polarization of DPH highly depends on its surrounding lipid microenvironment, which provides information about the microviscosity of the cell membrane.[34] As shown in Figure 5C, following the addition of cholesterol as a control, the membrane microviscosity in HepG2-P cells increased within 20 min, and it remained constant during the studied time, which was in agreement with the previous report.[35] In contrast, different concentrations of NOSC all showed the effect on reducing the microviscosity of the HepG2-P cell membrane, which was greater at the concentration close to or lower than its CMC compared with at the higher one.

Finally, the influences of NOSC on the intracellular GSH level and the activity of GST were estimated in HepG2-P cells. As shown in Figure 5D, the presence of NOSC revealed no remarkable impact on the intracellular amount of GSH or the activity of GST during 1 h of treatment regardless of the concentration of NOSC.

Cytotoxicity Studies. The *in vitro* cytotoxicity of different PTX formulations was evaluated on both HepG2 and HepG2-P cells using an MTT assay. Since we observed that the blank

dx.doi.org/10.1021/mp400340k | *Mol. Pharmaceutics* 2014, 11, 145−157

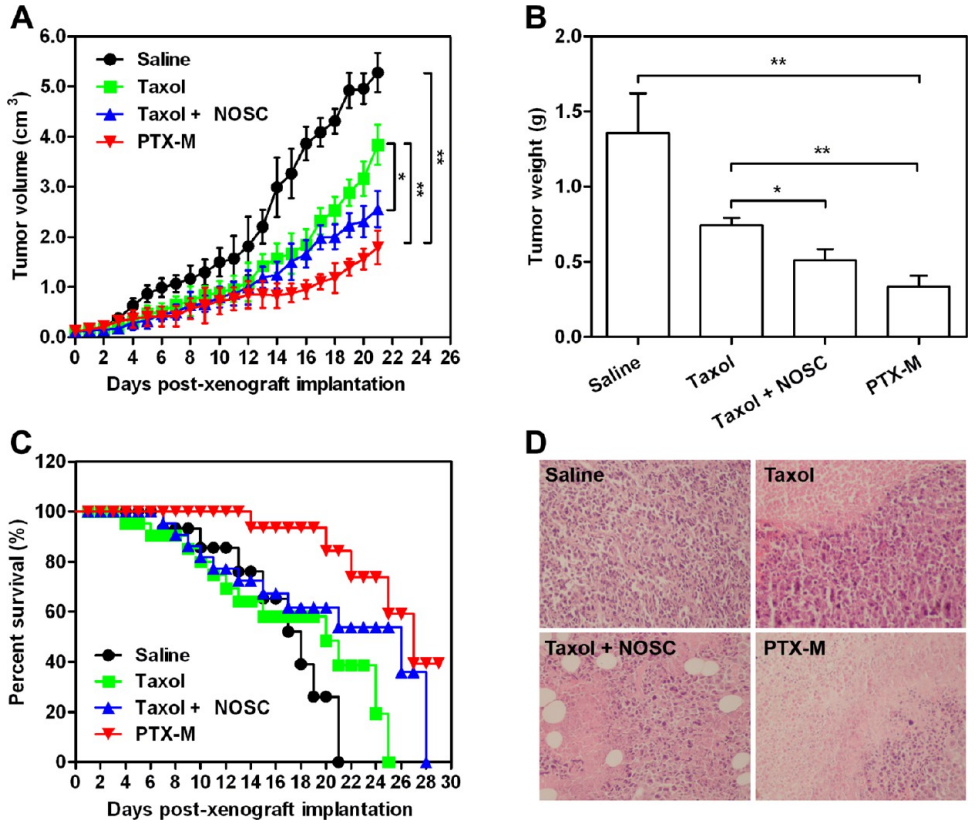

Figure 7. *In vivo* antitumor efficacy of different PTX formulations in the Heps-P tumor xenograft mice models. The tumor-bearing mice were intravenously injected by different PTX formulations at a PTX dose of 20 mg/kg at day 3, 5, 7, 9, and 11: the tumor growth curves during the treatments for 21 days (A), the weights of the tumors collected from the mice after the treatment at day 21 (B), Kaplan−Meier survival curves for 29 days (C), and H&E stained tumor sections after the treatment at day 21.

NOSC micelles did not show significant toxicity toward both HepG2 and HeG2-P cells (Figure S2, Supporting Information), the cytotoxicity of different PTX formulations here can be attributed to the release of free PTX molecules from the test groups. As shown in Figure 6 and Table 3, in HepG2 cells, all of the PTX formulations (PTX, Taxol, Taxol + NOSC, and PTX-M) displayed a concomitant increasing cytotoxicity with the increase of the PTX concentration. The IC_{50} values for 48 h was calculated to be 0.64 ± 0.04 μg/mL, 0.41 ± 0.02 μg/mL, 0.39 ± 0.03 μg/mL, and 0.30 ± 0.03 μg/mL, respectively. It was demonstrated that Taxol, Taxol + NOSC, and PTX-M performed an enhanced cytotoxicity compared to free PTX, and there was no evident difference among these three formulations. Furthermore, due to the prolonged incubation time, all of the IC_{50} values for 72 h of the PTX formulations were reduced, and PTX-M showed the highest cytotoxicity.

By comparison, in P-gp overexpressing HepG2-P cells, the IC_{50} value for 48 h of free PTX dramatically increased (16.39 ± 3.22 μg/mL), 24-fold higher than that in HepG2 cells (0.64 ± 0.04 μg/mL), which indicated that free PTX became less effective for PTX-resistant cancer treatment. Additionally, the cytotoxicity of free PTX toward HepG2-P cells did not elevate as the incubation time increased to 72 h, which was attributed to the high PTX resistance and sustained the efflux effect of HepG2-P cells. Taxol presented a greater cytotoxicity toward HepG2-P cells compared to free PTX, which had the 48 and 72 h IC_{50} values of 6.49 ± 1.14 μg/mL and 5.85 ± 0.72 μg/mL, respectively. The addition of NOSC significantly increased the cytotoxicity of Taxol, suggesting that NOSC could keep HepG2-P cells susceptible to PTX, thereby enhancing the cytotoxicity of Taxol in the MDR cancer cells.

The reversal effects of the formulations on the MDR cells were also represented in the form of resistance reversion index (RRI) shown in Table 3. In HepG2-P cells, Taxol with NOSC induced a much higher RRI than that without NOSC regardless of the incubation time. PTX-M exhibited a significantly improved cytotoxicity effect relative to other PTX formulations including PTX, Taxol, and Taxol + NOSC. Moreover, the 48 h IC_{50} value of PTX-M in HepG2-P cells showed the lowest value (0.55 ± 0.23 μg/mL), which was closed to that in HepG2 cells (0.30 ± 0.03 μg/mL). Furthermore, the IC_{50} value of PTX-M in HepG2-P cells for 72 h was lower than that for 48 h, implying that the effect of PTX-M on P-gp inhibition was not attenuated as the incubation time increased. It was worth noting that the RRI of PTX-M was 29.63 and 56.44 for 48 and 72 h, respectively, which were significantly higher than other studied PTX formulations.

Animal Studies. *In Vivo Antitumor Efficacy.* To evaluate the therapeutic efficacy of PTX-M *in vivo*, the antitumor activities of Taxol, Taxol + NOSC, and PTX-M were investigated in the Heps-P tumor-bearing mice. As shown in Figure 7A, all of the PTX formulations were effective in inhibiting the tumor growth compared to saline as a negative control. The tumor inhibition rate was in the order of PTX-M > Taxol + NOSC > Taxol. PTX-M was determined to have the optimal capability of suppressing the tumor growth. After the treatments, the tumor was excised and weighted, and the weights of tumor treated with saline, Taxol, Taxol + NOSC,

dx.doi.org/10.1021/mp400340k | *Mol. Pharmaceutics* 2014, 11, 145−157

and PTX-M were 1.35 ± 0.26 g, 0.74 ± 0.05 g, 0.51 ± 0.07 g, and 0.33 ± 0.08 g, respectively (Figure 7B). Based on this result, the inhibition rate (%) of tumor by these PTX formulations was calculated. Taxol containing Cremophpr EL, believed to inhibit a P-gp efflux pump, showed an inhibition rate (%) of 45.2%, which was in consistent with the earlier reports (44.4%).[34] Due to the PTX efflux inhibition function of NOSC, codelivery of Taxol and NOSC presented a obvious increase in the inhibition rate in the Heps-P tumor-bearing mice (63.2%). More importantly, the inhibition rate in mice receiving PTX-M was calculated to be 75.5%, sharply higher than that of Taxol (45.3%). These findings indicated that PTX-M expressed a greater therapeutic efficacy than Taxol with or without NOSC, which could be attributed to the combined effect of PTX-M mentioned above. Moreover, the survival of the Heps-P tumor-bearing mice after the treatment of different PTX formulations was described in a Kaplan−Meier plots as presented in Figure 7C. All of saline-treated mice were dead by 21 days, caused by the rapid growth of tumors. The survival time of Taxol and Taxol + NOSC-treated groups was 25 and 28 days, respectively, indicating that the enhanced therapeutic efficacy of Taxol could be induced by the addition of NOSC. In contrast, the survival of the mice treated with PTX-M is 40% at the end of the experiment (the 30th day), demonstrating the overwhelming antitumor activity of PTX-M than both Taxol and Taxol + NOSC as well as the prolonged survival time. Additionally, the histologic images of the H&E-stained tumor section displayed a massive cancer cell remission after the treatment of PTX-M (Figure 7D), providing substantial evidence of the efficient *in vivo* therapeutic activity of PTX-M.

Intratumoral Accumulation of PTX-M. To gauge the *in vivo* targetability of PTX-M, the intratumoral accumulation amount of PTX was assayed after intravenous administration of PTX-M into the Heps or Heps-P tumor-bearing mice. As shown in Figure 8, PTX-M presented the highest amount of PTX at the tumor site compared with Taxol and codelivery of Taxol with NOSC in both the Heps and the Heps-P tumor-bearing mice. PTX-M not only elevated the PTX accumulation in the tumor but also improved the intratumoral pharmacokinetic parameters (Table 4). In the Heps-P tumor-bearing mice, the area under the curve (AUC), the mean residence time (MRT), and the elimination half-life ($t_{1/2\beta}$) of PTX delivered by PTX-M were higher than that of other formulations, while the total body clearance (Cl) was lower. It was calculated that the AUC, MRT, $t_{1/2\beta}$, and Cl value for PTX-M was 4.3, 2.5, and 2.8-fold higher and 8.7-fold lower than that of the commercial Taxol, which further confirmed the feasibility of PTX-M for the application in cancer treatment.

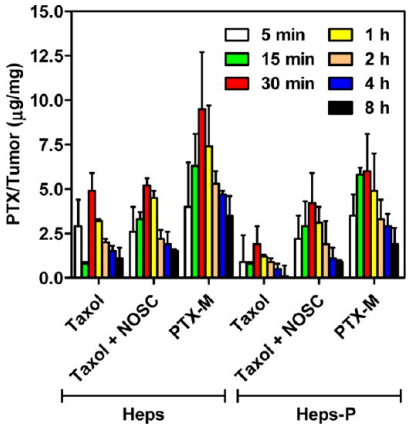

Figure 8. Accumulation amounts of PTX in the tumor tissues after intravenous injection of different PTX formulations into the Heps and Heps-P tumor-bearing mice at a PTX dose of 20 mg/kg.

Intratumoral Localization of PTX-M. To demonstrate the integrity of PTX-M accumulating at the tumor site by the enhanced permeability and retention (EPR) effect, double-labeled NOSC micelles were applied, in which a hydrophobic dye with red fluorescence, Nr, was coencapsulated with PTX to track the payloads, while FITC was covalently conjugated on NOSC polymer to track the carrier. The presence of Nr in the core of NOSC micelles presented no significant impact on the release of PTX from the micelles (Figure S3, Supporting Information). The intact Nr-loaded FITC-labeled NOSC micelles were observed as yellow fluorescence by the overlay between the red and green fluorescence. As shown in Figure 9, most of PTX-M remained its integrity in the tumor section, judged by a large part of the yellow fluorescence. A small part of micelles dissociated at the tumor site, which was determined by the separation between the green and the red fluorescence. It could be partly attributed to the dissociation of micelles and the release of Nr from PTX-M in the tumor tissues and cells.

DISCUSSION

Cellular Uptake Studies. *Effect of NOSC on the Cellular Uptake of PTX.* The increased cellular uptake of PTX in the presence of verapamil in HepG2 cells showed the P-gp inhibition effect *via* reducing ATPase activity.[5] The presence of Cremophor EL increased the cellular uptake of PTX in HepG2 cells at a low concentration but was inert at a high level. It has been reported that the nonionic surfactants (e.g., Cremophor EL and Tween 80) and the amphiphilic block copolymers (e.g., Pluronics) were able to inhibit P-gp by increasing the membrane fluidity[9] or restraining the drug efflux transporters by inhibiting ATPase in the tumor cells.[36,37] However, the greatest effect of the surfactants or polymer on P-gp inhibition was only at the concentration lower than their CMC.[22,38] The results in our work were consistent with the previous report that the greatest P-gp inhibition effect of Cremophor EL was found at the concentration no more than its CMC of 0.009% (w/v).[10] Of note, the mean cellular uptake of PTX in the presence of NOSC was comparable to (in HepG2 cells) or even higher than (in HepG2-P cells) that with the help of verapamil, which presented no obvious relationship with the concentration of NOSC. This high intracellular drug retention capability exhibits in a wide concentration range of NOSC from 0.008% to 0.04% to 0.08% (w/v), which were the concentrations lower than, equal to, and higher than its CMC of 0.045%.[26−28] It was implied that the enhancement of NOSC on the cellular uptake of PTX resulted from a unique mechanism other than that related to the surfactants and the Pluronic block copolymer.

Mechanisms of Cellular Uptake. The cellular uptake of the polymeric micelles commonly through an energy-dependent endocytosis, in which either a metabolic (e.g., low temperature at 4 °C)[39] or chemical energy inhibitor (e.g., sodium azide) can suppress the process. Due to the passive diffusion mechanism,[40] the cellular uptake of PTX in Taxol was insignificantly affected by both the metabolic and chemical energy inhibitors. In contrast, the remarkably decreased cellular uptake of PTX in PTX-M at 4 °C or in the presence of sodium azide 37 °C indicated that most of PTX-M was unable to enter the cells.

dx.doi.org/10.1021/mp400340k | *Mol. Pharmaceutics* 2014, 11, 145−157

Table 4. Pharmacokinetic Parameters of PTX after Intravenous Administration of Different PTX Formulations into the Heps and Heps-P Tumor-Bearing Mice

	pharmacokinetic parameters	Taxol	Taxol + NOSC	PTX-M
Heps	$AUC_{(0-8h)}$ (μg·h/g)	14.4 ± 0.84^b	18.2 ± 0.69	39.9 ± 0.32
	$MRT_{(0-8)}$ (h)	9.8 ± 0.38^b	14.8 ± 0.61	13.9 ± 0.91
	$t_{1/2\beta}$ (h)	7.1 ± 0.42^b	10.9 ± 0.75	9.9 ± 0.30
	Cl (mg/kg·h/(ug/g))	0.7 ± 0.14^b	0.5 ± 0.08	0.2 ± 0.16
Heps-P	$AUC_{(0-8h)}$ (μg·h/g)	4.7 ± 0.14	12.6 ± 0.72^b	24.9 ± 0.56^b
	$MRT_{(0-8)}$ (h)	2.9 ± 0.66	5.2 ± 0.84^a	10.2 ± 0.15^b
	$t_{1/2\beta}$ (h)	1.9 ± 0.39	3.5 ± 0.60^a	7.3 ± 0.76^b
	Cl (mg/kg·h/(ug/g))	3.9 ± 0.93	1.2 ± 0.18^a	0.4 ± 0.04^b

$^aP < 0.05$. $^bP < 0.01$, compared with Taxol in Heps-P tumor.

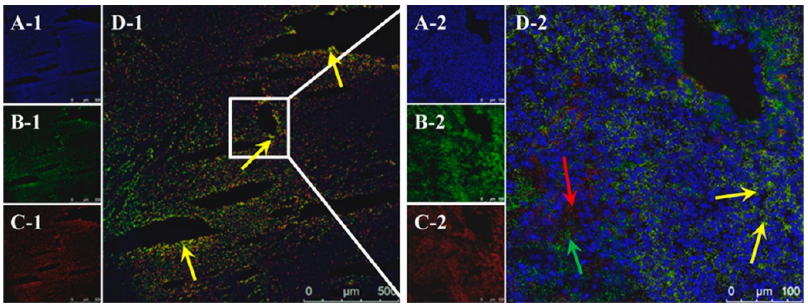

Figure 9. Intratumoral localization of FITC/Nr-M observed by CLSM at 8 h postinjection ito the Heps-P-bearing mice: blue-fluorescent nuclei stained by Hoechst (A), green-fluorescent FITC-labeled NOSC (FITC-NOSC) (B), red-fluorescent Nr (C), and overlay (D). Yellow, green, and red arrows indicate the intact PTX-M, FITC-NOSC, and Nr, respectively. A-2−D-2 are the magnified images of A-1−D-1, respectively.

The detected PTX amount could be due to the cytoadhesion of PTX-M on the cell membrane without the internalization.[41] It was confirmed that the cellular uptake of PTX-M was an energy-dependent endocytosis process, a general way for the internalization of micelles in many types of cells.[42] Based on this mechanism, the encapsulated PTX can enter the cells accompanied by the endocytosis of the NOSC micelles, which played an important role in protecting PTX *via* bypassing P-gp and therefore suppressing the efflux of PTX molecules by P-gp.

Kinetics of Cellular Uptake. In addition to the above effect of NOSC and its micelles on inhibiting P-gp and promoting the intracellular PTX accumulation, we aimed to investigate the dynamic process of drug transportation of PTX with the help of NOSC. The cellular uptake kinetics of Taxol, Taxol + NOSC (0.08%, w/v), and PTX-M were carried out in HepG2 and HepG2-P cells. PTX-M exhibited not only the highest level and speed of the cellular uptake but also the lowest drug efflux rate in both HepG2 and HepG2-P cells, which demonstrated that PTX in NOSC micelles experienced a rapid uptake and slow efflux process, thereby leading to the maintenance of a high concentration of PTX inside the cancer cells for a longer time.

According to these results in the cellular uptake studies above, we could draw a preliminary conclusion that the overperformance of PTX-M can be attributed to a combination of the inhibiting P-gp effect of NOSC and the bypassing P-gp action of intact PTX-M. To confirm this conclusion, two issues should be first clarified. One is the possible P-gp inhibition mechanism different from that of the surfactants and block copolymers. The other is the considerable evidence of PTX-M reaching the tumor cells as an intact form, which ensured the synergetic effect of NOSC micelles on the intracellular drug transportation and protection. Thus, the research on the P-gp inhibition mechanism of NOSC micelles and the *in vivo* antitumor activity of PTX-M has been carried out.

P-gp Inhibition Mechanism of NOSC Micelles. The P-gp inhibition mechanism of polymers is extremely complex, which involves the reduction of P-gp expression, the activity regulation of P-gp ATP enzyme, the interference of substrate recognition, and changes in the cellular membrane fluidity. To explore the potential P-gp inhibition mechanism of NOSC micelles, the influence of NOSC was investigated on the expression of P-gp, the activity of P-gp ATPase, the binding site of PTX on P-gp, the fluidity of cell membrane, the intracellular amount of GSH, and the activity of GST. NOSC had an insignificant impact on the expression of P-gp that was located in the cell membrane, which indicated that the anti-P-gp efflux mechanism of NOSC is not related to the inhibition of P-gp expression. Similar to verapamil, NOSC at different concentrations can stimulate the activity of P-gp ATPase. Additionally, the binding assay of PTX in the presence of NOSC confirmed that NOSC was a competitive substrate of P-gp against PTX, which was able to directly interact with P-gp on a putative site near or coincident with the PTX-binding site. A similar mechanism has been reported in the case of liposomes that interfere with the binding of vincristine in the cells over-expressing P-gp.[43,44] This mechanism was believed in connection to the occupation of glycine 185, a critical residue for the direct binding and inhibitory site of P-gp using an anionic liposome (Lipodox).[45] Furthermore, NOSC at different concentrations could decrease the microviscosity of the cell membrane, whereas it did not influence the intercellular GSH/GST level. Based on these findings, it could be deduced that the multiple mechanisms were involved in the P-gp inhibition effect of NOSC, such as stimulating P-gp ATPase, competitively impeding the binding of PTX with P-gp and reducing the fluidity of the cell membrane.

Cytotoxicity Studies. Compared with free PTX, Taxol, and Taxol + NOSC, PTX-M was determined to have the

highest cytotoxicity toward both HepG2 and HepG2-P cells. Unlike other PTX formulations, the cell type and the incubation time showed no remarkable influence on the cytotoxicity of PTX-M, which suggested that the PTX-M formulation almost enabled PTX to ignore the effect of P-gp-induced efflux and retain the sensitivity of the MDR cells to PTX. Collectively, HepG2-P cells were more susceptible to PTX-M, which could be a promising DDS for the superior treatment of the MDR solid tumors.

Animal Studies. *In Vivo Antitumor Efficacy.* Compared to Taxol, the enhanced tumor inhibition of the Taxol + NOSC group was attributed to the P-gp inhibition function of the NOSC polymer. The highest tumor growth inhibition efficacy of PTX-M was mainly explained by a combination effect: (1) enhanced accumulation of PTX at the tumor site by the EPR effect of PTX-M; (2) improved cellular uptake of PTX *via* endocytosis of PTX-M; (3) sustained release of PTX from PTX-M inside the cells; (4) persistent P-gp inhibition effect by NOSC polymer and its micelles. The increased amount of PTX that delivered at the tumor site and transported into tumor cells by the combined functions of NOSC micelles produced an elevated local PTX concentration and prolonged the resistance time of PTX in the tumor cells. This conclusion could be validated by the following quantitative studies of PTX concentration and localization of PTX-M in the tumor tissues.

Intratumoral Accumulation of PTX-M. PTX-M showed the highest drug concentration among all of the test PTX formulations regardless of the type of cells, which was also demonstrated to have improved pharmacokinetic parameters compared to Taxol and codelivery of Taxol with NOSC (0.08%, w/v). It was indicated that PTX-M could enhance the concentration and prolong the resistance time of PTX in the tumor, which was mainly due to the efficient passive tumor-targeting capability of PTX-M in an intact form after intravenous administration and the subsequent cellular uptake *via* an endocytosis pathway in the tumor tissues. Furthermore, the increased AUC, MRT, $t_{1/2\beta}$, and decreased Cl values of PTX-M indicated that the PTX in NOSC micelles inside the tumor cells could be sustainedly released from the NOSC micelles, which might reduce the drug efflux *via* the protection and competitive binding of NOSC polymer and its micelles.

Intratumoral Localization of PTX-M. According to the results above, it was confirmed that PTX-M enabled the high PTX accumulation in HepG2-P cells as well as the Heps-P tumor tissue and therefore improved the therapeutic efficacy of PTX in the Heps-P tumor-bearing mice. A preliminary conclusion could be drawn that this overperformed efficacy was closely related to the realization of the tumor targeting of PTX-M in an intact form after intravenous administration. To validate this presumption, the study on the intratumor localization of PTX-M has been carried out. The CLSM images showed that the double-fluorescence-labeled PTX-M following intravenous injection was delivered at the tumor site mainly in the form of the intact drug-loaded NOSC micelles, which was different from the previous literature reporting that the anticancer drug and block copolymer was delivered separately to the solid tumor after intravenous injection of DOX-Pluronic L61/Pluronic F127 mixed micelles.[46,47] It was confirmed that the inherent and different drug delivery behavior of PTX-M as well as the superior P-gp inhibition effect of NOSC resulted in the improvement of the *in vivo* therapeutic efficacy for cancer treatment.

CONCLUSIONS

To overcome the relapse of human tumors caused by the MDR phenomenon, the investigations of PTX-M on the *in vitro* cellular uptake, the *in vivo* antitumor efficiency, and the P-gp inhibition mechanism have been performed in both HepG2 and PTX-resistant HepG2-P cells as well as their tumor xenograft mice models, compared to free PTX, Taxol, and codelivery of Taxol with NOSC. PTX-M was able to enhance the accumulation and prolong the residence time of PTX in the tumor tissue, due to the P-gp inhibition effect of NOSC and the excellent properties of its micelles. The former was determined to be a multiple mechanism of stimulating P-gp ATPase, competitively impeding the binding of PTX with P-gp and reducing the fluidity of the cell membrane by NOSC polymer and its micelles. The latter was confirmed to be associated with the high drug-loading efficiency, stability, tumor targetability, and the effective intracellular delivery of PTX-M. Taken together, the results in this work suggested that PTX-M might be a promising applicable device for overcoming PTX resistance in cancer treatment.

ASSOCIATED CONTENT

Supporting Information

Details of the structure of NOSC, the preparation of PTX-M, the *in vitro* cytoxicity of NOSC toward HepG2 and HepG2-P cells, and the *in vitro* release of PTX from PTX-M. This material is available free of charge via the Internet at http://pubs.acs.org.

AUTHOR INFORMATION

Corresponding Authors

*Tel.: +86 25 83271171. Fax: +86 25 83271171. E-mail: zhangcancpu1801@163.com.

*E-mail: ayanju@163.com.

Author Contributions

X.J. and R.M. contributed equally to this work.

Notes

The authors declare no competing financial interest.

ACKNOWLEDGMENTS

This work was supported by the National Natural Science Foundation of China (81072589, 81273468), the Project Program of State Key Laboratory of Natural Medicines, China Pharmaceutical University (SKLNMZZ201206, SKLNMZZCX201306), and 111 Project from the Ministry of Education of China and the State Administration of Foreign Expert Affairs of China (no. 111-2-07).

REFERENCES

(1) Gottesman, M. M.; Pastan, I. Biochemistry of multidrug resistance mediated by the multidrug transporter. *Annu. Rev. Biochem.* **1993**, *62*, 385−427.

(2) Gottesman, M. M. Mechanisms of cancer drug resistance. *Annu. Rev. Med.* **2002**, *53*, 615−627.

(3) Gottesman, M. M.; Fojo, T.; Bates, S. E. Multidrug resistance in cancer: role of ATP-dependent transporters. *Nat. Rev. Cancer* **2002**, *2*, 48−58.

(4) Pérez-Sayáns, M.; Somoza-Martín, J. M.; Barros-Angueira, F.; Diz, P. G.; Rey, J. M.; García-García, A. Multidrug resistance in oral squamous cell carcinoma: The role of vacuolar ATPases. *Cancer Lett.* **2010**, *295*, 135−143.

(5) Wang, F.; Zhang, D.; Zhang, Q.; Chen, Y.; Zheng, D.; Hao, L.; Duan, C.; Jia, L.; Liu, G.; Liu, Y. Synergistic effect of folate-mediated

targeting and verapamil-mediated P-gp inhibition with paclitaxel -polymer micelles to overcome multi-drug resistance. *Biomaterials* **2011**, *32*, 9444−9956.
(6) Daoudaki, M.; Fouzas, I.; Stapf, V.; Ekmekcioglu, C.; Imvrios, G.; Andoniadis, A.; Demetriadou, A.; Thalhammer, T. Cyclosporine a augments P-glycoprotein expression in the regenerating rat liver. *Biol. Pharm. Bull.* **2003**, *26*, 303−307.
(7) van Asperen, J.; van Tellingen, O.; van der Valk, M. A.; Rozenhart, M.; Beijnen, J. H. Enhanced oral absorption and decreased elimination of paclitaxel in mice cotreated with cyclosporin A. *Clin. Cancer Res.* **1998**, *4*, 2293−2297.
(8) Liu, Y.; Huang, L.; Liu, F. Paclitaxel nanocrystals for overcoming multidrug resistance in cancer. *Mol. Pharmaceutics* **2010**, *7*, 863−869.
(9) Rege, B. D.; Kao, J. P.; Polli, J. E. Effects of nonionic surfactants on membrane transporters in Caco-2 cell monolayers. *Eur. J. Pharm. Sci.* **2002**, *16*, 237−246.
(10) Shono, Y.; Nishihara, H.; Matsuda, Y.; Furukawa, S.; Okada, N.; Fujita, T.; Yamamoto, A. Modulation of intestinal P-glycoprotein function by cremophor EL and other surfactants by an in vitro diffusion chamber method using the isolated rat intestinal membranes. *J. Pharm. Sci.* **2004**, *93*, 877−885.
(11) Brigger, I.; Dubernet, C.; Couvreur, P. Nanoparticles in cancer therapy and diagnosis. *Adv. Drug Delivery Rev.* **2002**, *54*, 631−651.
(12) Palakurthi, S.; Yellepeddi, V. K.; Vangara, K. K. Recent trends in cancer drug resistance reversal strategies using nanoparticles. *Expert Opin. Drug Delivery* **2012**, *9*, 287−301.
(13) Chavanpatil, M. D.; Patil, Y.; Panyam, J. Susceptibility of nanoparticle-encapsulated paclitaxel to P-glycoprotein-mediated drug efflux. *Int. J. Pharmaceutics* **2006**, *320*, 150−156.
(14) Gatouillat, G.; Odot, J.; Balasse, E.; Nicolau, C.; Tosi, P. F.; Hickman, D. T.; López-Deber, M. P.; Madoulet, C. Immunization with liposome-anchored pegylated peptides modulates doxorubicin sensitivity in P-glycoprotein-expressing P388 cells. *Cancer Lett.* **2007**, *257*, 165−171.
(15) Yokoyama, M. Polymeric micelles as a new drug carrier system and their required considerations for clinical trials. *Expert Opin. Drug Delivery* **2010**, *7*, 145−158.
(16) Kabanov, A. V.; Batrakova, E. V.; Alakhov, V. Y. Pluronic block copolymers as novel polymer therapeutics for drug and gene delivery. *J. Controlled Release* **2002**, *82*, 189−212.
(17) Batrakova, E. V.; Kelly, D. L.; Li, S.; Li, Y.; Yang, Z.; Xiao, L.; Alakhova, D. Y.; Sherman, S.; Alakhov, V. Y.; Kabanov, A. V. Alteration of genomic responses to doxorubicin and prevention of MDR in breast cancer cells by a polymer excipient: pluronic P85. *Mol. Pharmaceutics* **2006**, *3*, 113−123.
(18) Kabanov, A. V.; Batrakova, E. V.; Alakhov, V. Y. Pluronic block copolymers for overcoming drug resistance in cancer. *Adv. Drug Delivery Rev.* **2002**, *54*, 759−779.
(19) Batrakova, E. V.; Li, S.; Vinogradov, S. V.; Alakhov, V. Y.; Miller, D. W.; Kabanov, A. V. Mechanism of pluronic effect on P-glycoprotein efflux system in blood-brain barrier: contributions of energy depletion and membrane fluidization. *J. Pharmacol. Exp. Ther.* **2001**, *299*, 483−93.
(20) Alvarez-Lorenzo, C.; Sosnik, A.; Concheiro, A. PEO-PPO block copolymers for passive micellar targeting and overcoming multidrug resistance in cancer therapy. *Curr. Drug. Targets* **2011**, *12*, 1112−1130.
(21) Diao, Y. Y.; Li, H. Y.; Fu, Y. H.; Han, M.; Hu, Y. L.; Jiang, H. L.; Tsutsumi, Y.; Wei, Q. C.; Chen, D. W.; Gao, J. Q. Doxorubicin-loaded PEG-PCL copolymer micelles enhance cytotoxicity and intracellular accumulation of doxorubicin in adriamycin-resistant tumor cells. *Int. J. Nanomed.* **2011**, *6*, 1955−1962.
(22) Shono, Y.; Nishihara, H.; Matsuda, Y.; Furukawa, S.; Okada, N.; Fujita, T.; Yamamoto, A. Modulation of intestinal P-glycoprotein function by cremophor EL and other surfactants by an in vitro diffusion chamber method using the isolated rat intestinal membranes. *J. Pharm. Sci.* **2004**, *93*, 877−885.
(23) Katneni, K.; Charman, S. A.; Porter, C. J. Impact of cremophor-EL and polysorbate-80 on digoxin permeability across rat jejunum: delineation of thermodynamic and transporter related events using the reciprocal permeability approach. *J. Pharm. Sci.* **2007**, *96*, 280−293.
(24) Gelderblom, H.; Verweij, J.; Nooter, K.; Sparreboom, A. Cremophor EL: the drawbacks and advantages of vehicle selection for drug formulation. *Eur. J. Cancer* **2001**, *37*, 1590−1598.
(25) Nyman, D. W.; Campbell, K. J.; Hersh, E.; Long, K.; Richardson, K.; Trieu, V.; Desai, N.; Hawkins, M. J.; Von Hoff, D. D. Phase I and pharmacokinetics trial of ABI-007, a novel nanoparticle formulation of paclitaxel in patients with advanced nonhematologic malignancies. *J. Clin. Oncol.* **2005**, *23*, 7785−7793.
(26) Zhang, C.; Qu, G.; Sun, Y.; Wu, X.; Yao, Z.; Guo, Q.; Ding, Q.; Yuan, S.; Shen, Z.; Ping, Q.; Zhou, H. Pharmacokinetics, biodistribution, efficacy and safety of N-octyl-O-sulfate chitosan micelles loaded with paclitaxel. *Biomaterials* **2008**, *29*, 1233−1241.
(27) Mo, R.; Xiao, Y.; Sun, M.; Zhang, C.; Ping, Q. Enhancing effect of N-octyl-O-sulfate chitosan on etoposide absorption. *Int. J. Pharmaceutics* **2011**, *409*, 38−45.
(28) Mo, R.; Jin, X.; Li, N.; Ju, C.; Sun, M.; Zhang, C.; Ping, Q. The mechanism of enhancement on oral absorption of paclitaxel by N-octyl-O-sulfate chitosan micelles. *Biomaterials* **2011**, *32*, 4609−4620.
(29) Mechetner, E. B.; Roninson, I. B. Efficient inhibition of P-glycoprotein-mediated multidrug resistance with a monoclonal antibody. *Proc. Natl. Acad. Sci. U.S.A.* **1992**, *89*, 5824−5828.
(30) Shinitzky, M.; Barenholtz, Y. Dynamics of the hydrocarbon layer in liposomes of lecithin and sphingomyelin containing dicetylphosphate. *J. Biol. Chem.* **1974**, *249*, 2652−2657.
(31) Ford, J. M. Experimental reversal of P-glycoprotein-mediated multidrug resistance by pharmacological chemosensitisers. *Eur. J. Cancer* **1996**, *32A*, 991−1001.
(32) Ambudkar, S. V.; Dey, S.; Hrycyna, C. A.; Ramachandra, M.; Pastan, I.; Gottesman, M. M. Biochemical, cellular, and pharmacological aspects of the multidrug transporter. *Annu. Rev. Pharmacol. Toxicol.* **1999**, *39*, 361−398.
(33) Roozemond, R. C.; Urli, D. C. Lipid composition and microviscosity of subcellular fractions from rabbit thymocytes. Differences in the microviscosity of plasma membranes from subclasses of thymocytes. *Biochim. Biophys. Acta* **1979**, *556*, 17−37.
(34) Plaèsíek, J.; Jarolim, P. Interaction of the fluorescent probe 1,6-diphenyl-1,3,5-hexatriene with biomembranes. *Gen. Physiol. Biophys.* **1987**, *6*, 425−437.
(35) Wang, Y.; Hao, J.; Li, Y.; Zhang, Z.; Sha, X.; Han, L.; Fang, X. Poly(caprolactone)-modified Pluronic P105 micelles for reversal of paclitaxcel-resistance in SKOV-3 tumors. *Biomaterials* **2012**, *33*, 4741−4751.
(36) Alakhov, V. Yu.; Moskaleva, E. Yu.; Batrakova, E. V.; Kabanov, A. V. Hypersensitization of multidrug resistant human ovarian carcinoma cells by pluronic P85 block copolymer. *Bioconjugate Chem.* **1996**, *7*, 209−216.
(37) Rapoport, N.; Marin, A.; Luo, Y.; Prestwich, G. D.; Muniruzzaman, M. D. Intracellular uptake and trafficking of Pluronic micelles in drug-sensitive and MDR cells: effect on the intracellular drug localization. *J. Pharm. Sci.* **2002**, *91*, 157−170.
(38) Batrakova, E.; Lee, S.; Li, S.; Venne, A.; Alakhov, V.; Kabanov, A. Fundamental relationships between the composition of pluronic block copolymers and their hypersensitization effect in MDR cancer cells. *Pharm. Res.* **1999**, *16*, 1373−1379.
(39) Hu, Y.; Litwin, T.; Nagaraja, A. R.; Kwong, B.; Katz, J.; Watson, N.; Irvine, D. J. Cytosolic delivery of membrane-impermeable molecules in dendritic cells using pH-responsive core-shell nanoparticles. *Nano Lett.* **2007**, *7*, 3056−3064.
(40) Walle, U. K.; Walle, T. Taxol transport by human intestinal epithelial Caco-2 cells. *Drug Metab. Dispos.* **1998**, *26*, 343−346.
(41) Win, K. Y.; Feng, S. S. Effects of particle size and surface coating on cellular uptake of polymeric nanoparticles for oral delivery of anticancer drugs. *Biomaterials* **2005**, *26*, 2713−2722.
(42) Zeng, X.; Zhang, Y.; Nyström, A. M. Endocytic uptake and intracellular trafficking of bis-MPA-based hyperbranched copolymer micelles in breast cancer cells. *Biomacromolecules* **2012**, *13*, 3814−3822.

(43) Rahman, A.; Husain, S. R.; Siddiqui, J.; Verma, M.; Agresti, M.; Center, M.; Safa, A. R.; Glazer, R. I. Liposome-mediated modulation of multidrug resistance in human HL-60 leukemia cells. *J. Natl. Cancer Inst.* **1992**, *84*, 1909−1915.
(44) Thierry, A. R.; Dritschilo, A.; Rahman, A. Effect of liposomes on P-glycoprotein function in multidrug resistant cells. *Biochem. Biophys. Res. Commun.* **1992**, *187*, 1098−1105.
(45) Riganti, C.; Voena, C.; Kopecka, J.; Corsetto, P. A.; Montorfano, G.; Enrico, E.; Costamagna, C.; Rizzo, A. M.; Ghigo, D.; Bosia, A. Liposome-encapsulated doxorubicin reverses drug resistance by inhibiting P-glycoprotein in human cancer cells. *Mol. Pharmaceutics* **2011**, *8*, 683−700.
(46) Danson, S.; Ferry, D.; Alakhov, V.; Margison, J.; Kerr, D.; Jowle, D.; Brampton, M.; Halbert, G.; Ranson, M. Phase I dose escalation and pharmacokinetic study of pluronic polymer-bound doxorubicin (SP1049C) in patients with advanced cancer. *Br. J. Cancer* **2004**, *90*, 2085−2091.
(47) Kabanov, A. V.; Batrakova, E. V.; Alakhov, V. Y. An essential relationship between ATP depletion and chemosensitizing activity of Pluronic block copolymers. *J. Controlled Release* **2003**, *91*, 75−83.